Analysis of Morphological Changes of Lamina Cribrosa Under Acute Intraocular Pressure Change

Mathilde Ravier[1(✉)], Sungmin Hong[1], Charly Girot[2], Hiroshi Ishikawa[3], Jenna Tauber[3], Gadi Wollstein[3], Joel Schuman[3], James Fishbaugh[1], and Guido Gerig[1]

[1] Department of Computer Science, Tandon School of Engineering, Brooklyn, NY, USA
{mor244,gerig}@nyu.edu
[2] Department of Computer Science, CPE Lyon School of Engineering, Lyon, France
[3] Department of Ophthalmology, Langone Medical Center, New York City, NY, USA

Abstract. Glaucoma is the second leading cause of blindness worldwide. Despite active research efforts driven by the importance of diagnosis and treatment of the optic degenerative neuropathy, the relationship between structural and functional changes along the glaucomateous evolution are still not clearly understood. Dynamic changes of the lamina cribrosa (LC) in the presence of intraocular pressure (IOP) were suggested to play a significant role in optic nerve damage, which motivates the proposed research to explore the relationship of changes of the 3D structure of the LC collagen meshwork to clinical diagnosis. We introduce a framework to quantify 3D dynamic morphological changes of the LC under acute IOP changes in a series of swept-source optical coherence tomography (SS-OCT) scans taken under different pressure states. Analysis of SS-OCT images faces challenges due to low signal-to-noise ratio, anisotropic resolution, and observation variability caused by subject and ocular motions. We adapt unbiased diffeomorphic atlas building which serves multiple purposes critical for this analysis. Analysis of deformation fields yields desired global and local information on pressure-induced geometric changes. Deformation variability, estimated with repeated images of a healthy volunteer without IOP elevation, is found to be a magnitude smaller than pressure-induced changes and thus illustrates feasibility of the proposed framework. Results in a clinical study with healthy, glaucoma suspect, and glaucoma subjects demonstrate the potential of the proposed method for non-invasive in vivo analysis of LC dynamics, potentially leading to early prediction and diagnosis of glaucoma.

1 Introduction

Glaucoma is the second leading cause of blindness and visual morbidity worldwide [9]. The optic degenerative neuropathy, characterized by a high eye pressure that damages the optic nerve, is challenging to treat as it has no apparent

A. F. Frangi et al. (Eds.): MICCAI 2018, LNCS 11071, pp. 364–371, 2018.
https://doi.org/10.1007/978-3-030-00934-2_41

symptoms before vision loss. Because damage is irreversible, timely diagnosis of disease and tracking its progression are of paramount importance. Structural deformation of the lamina cribrosa (LC), a connective tissue located in the optic nerve head, is suggested to play an important role in glaucomateous damage [4]. The LC is a collagen meshwork where all retinal axons pass through to the brain. Despite the importance of analyzing structural changes of the LC, there has not been any previous study analyzing full 3D changes of the LC which would give clinicians new insight into the pathology of the disease.

Previous studies of the LC structure generally used *ex vivo* or animals experiments [6,10]. Recently, with the progress of swept-source optical coherence tomography (SS-OCT), a few studies made use of the microscopic resolution imaging of the *in vivo* human LC. Previous studies showed promising results on 3D SS-OCT images for structural analysis of the LC, but results required extensive manual interactions and had aspects of the analysis limited to 2D [7,12], impeded by challenges in SS-OCT imaging such as scan variability due to subject and ocular motions, low signal-to-noise ratio, and an anisotropic voxel size [8]. In [3], a computational framework was proposed to analyze the deformation of the LC but analysis was limited to a single case without a validation study.

In this paper, we propose an unified framework to characterize morphological changes of micro-structures of the human LC *in vivo* by carefully selecting image analysis approaches to tackle the major challenges. This includes image denoising [2], image resampling [11], rigid alignment, and deformation-based analysis. The methodology is tested and validated in intraocular (IOP) experiments for comparative analysis between normal, glaucoma suspect, and glaucoma subjects.

We adopt unbiased diffeomorphic atlas building [5] to construct subject-specific LC atlases, which results in a deformable mapping of the series of pressure-state images to study pressure induced 3D structural changes of the LC, and to quantify delicate interactions of the LC micro-structures as a function of pressure. Variability of imaging and image analysis is assessed with repeated scans of a healthy volunteer without pressure.

2 Methods

2.1 IOP Experiment Setup

To analyze the structural changes induced by IOP elevation, an ophthalmodynamometer device was used to apply controlled pressure on the temporal sclera. Anesthetized eyes were imaged twice at baseline, 30g load of ophthalmodynamometer, and recovery after five minutes from IOP elevation. All subjects were scanned with a prototype SS-OCT system. Each 3D volume has a field-of-view of $3.5 \times 3.5 \times 1.6\text{mm}^3$ with $400 \times 400 \times 861$ voxel resolution. Clinical experts first assessed data quality to exclude severely corrupted images after intra-volume motion artifact correction and also images where the LC area was not fully visible.

2.2 Image Preprocessing

Image Resampling: Images from the prototype SS-OCT imaging system have anisotropic voxel dimensions, $8.75 \times 1.86 \times 8.75\ \mu m^3$. This anisotropy may lead to incorrect results from 3D image processing methods which assume isotropic voxel grids. We applied B-spline image resampling [11] to up-sample images to an isotropic $2 \times 2 \times 2\ \mu m^3$ voxel grid.

Noise Reduction: In order to overcome the speckle noise pattern inherent in OCT images, we make use of previously reported results in [3] where six filtering methods for OCT images were tested and compared. We therefore applied the best performing method, the block matching and 3D filtering (BM3D) method [2]. BM3D is based on a collaborative Wiener filtering on 3D groups of 2D image segments. This method preserves detail in local structures in images while reducing speckle noise.

Rigid Intrasubject Image Alignment: One major challenge of the analysis is to cope with patient and intra-ocular motions over the longitudinal series of scans and also scanning variability. Second, the SS-OCT images have a large field of view which covers the entire area of the optic nerve head. To constrain the analysis to the LC, images of a subject were rigidly aligned to correct for motion, and cropped to a region-of-interest of the LC area. Clinical experts define the best quality baseline image as a target reference for rigid alignment of the series.

2.3 Unbiased Atlas Building

To capture dynamic 3D structural changes, we adopt an unbiased diffeomorphic atlas building method [1,5] to create an atlas of each pressure state, baseline, IOP elevation (30 $mmHg$), and post pressure recovery, and finally an overall subject-specific atlas. Here, we follow a two-step procedure to overcome low SNR of high-resolution images from the experimental OCT device. For each of the three pressure states, a pressure specific template was estimated from two repeated scans. These pressure specific templates then form the basis for estimating a subject-specific unbiased atlas (Fig. 1). This two-step procedure enables us to improve the image quality of each pressure state under assumption that structural property of same pressure state is homogeneous.

The diffeomorphisms h_1, h_2, and h_3 that map the pressure state averages to the template encode the structural changes as deviations from average. Also, the inverse of $\mathbf{h}$ will be used to map structural information extracted from the atlas to each pressure state, e.g. masking of the LC area. Deformations from baseline to different pressure states are computed directly by composition of diffeomorphisms. For example, deformation from baseline to IOP elevation $\phi_{IOP} = h_2^{-1} \circ h_1$ and from baseline to recovery $\phi_{recovery} = h_3^{-1} \circ h_1$ were finally used for comparative analysis between clinical groups.

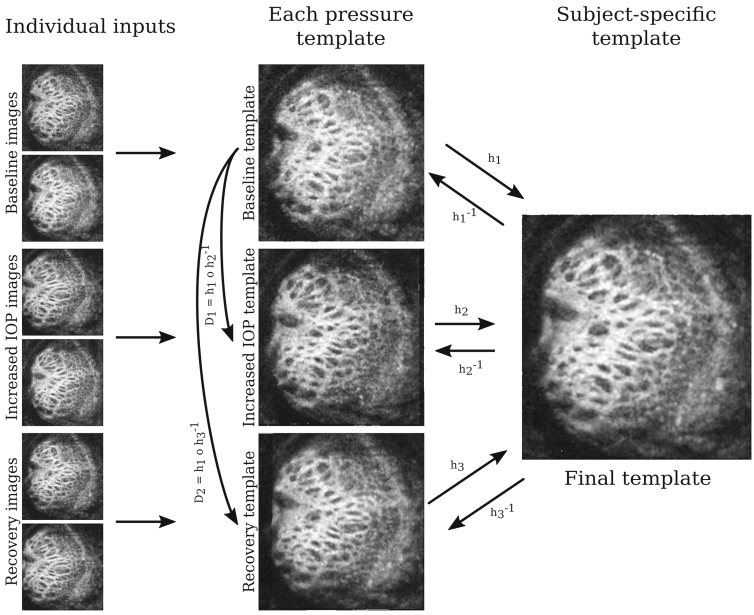

Fig. 1. Overview of subject-specific template construction. Repeated images for each pressure state are used to estimated pressure specific templates, which are used in turn to estimate the final template. Deformations between pressure state averages are calculated by composition of diffeomorphisms.

3 Results

3.1 Validation

We first assessed the stability and repeatability of our method using repeated SS-OCT images. Thirteen repeated scans of a healthy volunteer were acquired.

Scanning Stability: There is inherent scanning variability of the prototype SS-OCT imaging even for the same subject under patient's eyes during scanning and alignment of eyes to an OCT imaging sensor relies on manual adjustment by a technician. To analyze variability of SS-OCT scans, we estimated a template utilizing all 13 images and calculated the magnitude of deformation from template to each image. The deformation can be considered as the square root of Fréchet variance analogous to standard deviation of a scalar data. The Fréchet variance calculated the geometrical variance of all 13 images from a same subject at same baseline state to show the inherent variability of SS-OCT image scans at a same condition.

This study showed low magnitude (mean of 0.006 ± 0.003 mm) of deformation and consistent deformation distribution, indicating that the LC structure in each imaged LC is similar.

Framework Stability: We further assess stability by mimicking the IOP experiment using images from the healthy volunteer under no external pressure, to establish baseline performance without the added complexity of subject variability and pressure changes. From the 13 images, we randomly selected 6 and randomly assigned them to "pressure states" (2 each). This process is repeated 10 times. "Pressure" specific templates and overall templates are estimated as before (Sect. 2.3). Thus, in this validation experiment, the magnitude of deformation represents structural changes due only to scanning variability or ambiguity introduced by our processing.

The average magnitude of deformation of all sets was 0.007 mm with standard deviation 0.003 mm. Mean and standard deviation show that the magnitude of deformation is lower than the one caused by IOP elevation (0.014 ± 0.006 mm). It also shows that the deformation of recovery images (0.009 ± 0.004 mm) from baseline images are in a range of the deformations of the repeated scans.

3.2 Clinical Study

Twenty-two subjects, two healthy, twelve glaucoma, and eight suspect (structural changes in anatomy without vision loss), were scanned using the swept source 3D OCT system. Each subject was imaged as follows: 2 scans at baseline, at increased IOP ($30\ mmHg$) induced by an ophthalmodynameter, at post pressure, after 5 min of recovery. All images underwent an expert quality control where scans corrupted by motion were excluded. When two scans at each pressure state were not available after the quality control, we used a single image in place of a pressure specific template. For both global and local analysis, we used the deformation fields to quantify the deformation that maps the three pressure states into correspondence. Those deformation fields were estimated by composition of the diffeomorphic maps that transform every input image to the average in the template construction.

Global Analysis: Distribution of Deformation Magnitude. To study the global behavior of the LC structure, we calculated the magnitude of deformation from baseline to increased IOP and from baseline to recovery for every subject. We restricted those deformations by masking them to the visible LC only. The results were visualized with histograms.

We plot the distribution of deformation magnitudes integrated over the LC volume to compare changes at different pressure states. Figure 2 illustrates the examples of single subjects from healthy and glaucoma groups. Those subjects show a larger deformation for IOP (in yellow) than for post pressure recovery (in purple). Among the 22 subjects, 21 showed this pattern.

We also compared the distribution of deformation magnitude of all subjects at elevated IOP and studied the distributions of the means of deformation. Figure 3 illustrates those results with respect to the three groups. Due to the limited sample size, the comparison at elevated IOP between the different groups does not lead to any clinical conclusion. However, we can clearly see that elevated IOP has a larger deformation than recovery over the groups (left side figure). This

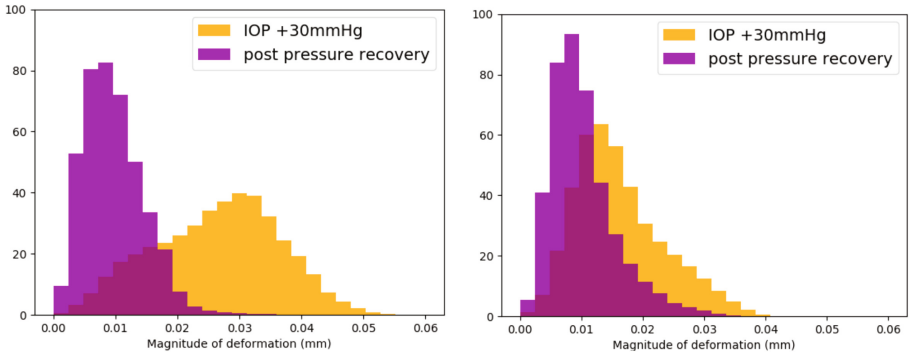

(a) Healthy (b) Glaucoma

Fig. 2. Single subject examples. Histograms represent distribution of the magnitude of deformation at elevated IOP (yellow) and post pressure recovery (purple) for a healthy and a glaucoma subject. Both subjects show larger deformation at elevated IOP than at recovery.

indicates that the experimental setup and analysis methodology are sensitive to tissue response to pressure and may serve as an *in-vivo* diagnostic or monitoring procedure well suited for routine clinical practice.

Table 1 represents the means of the deformations and their standard deviations for healthy, glaucoma suspect, and glaucoma subjects at elevated IOP and recovery. The healthy group shows a larger difference between elevated IOP and recovery than the other groups. This may indicate that the LC becomes stiffer when glaucoma appears.

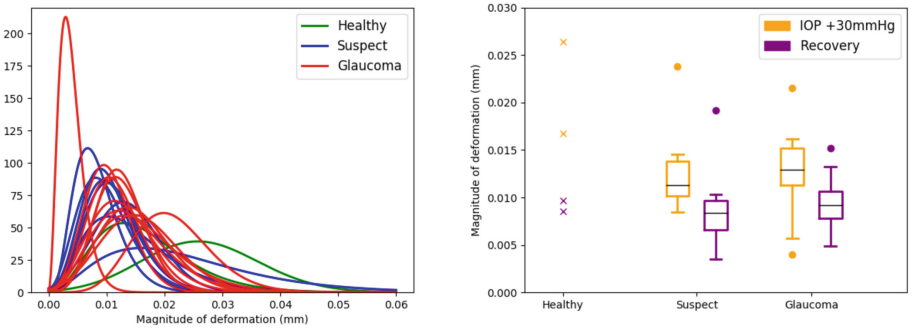

Fig. 3. Group-wise study. Left) Comparison of the distribution of deformation magnitude at elevated IOP for all subjects (green: healthy, blue: suspect, red: glaucoma). Right) The shape of the distribution of the means of deformation magnitude by groups of subjects. Elevated IOP and recovery statistics are represented in yellow and purple, respectively. The healthy group is being composed of two subjects so that the statistics is displayed as dots.

Table 1. Means and standard deviations of deformation magnitude (in mm) per groups of subjects and per pressure states.

Group	Pressure	
	IOP +30 $mmHg$	Recovery
Healthy	0.0216 ± 0.009	0.0091 ± 0.005
Suspect	0.0129 ± 0.006	0.0089 ± 0.004
Glaucoma	0.0128 ± 0.005	0.0095 ± 0.005

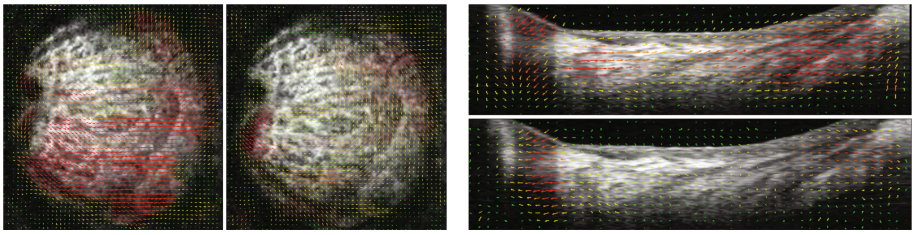

(a) En face views (b) Cross-section views

Fig. 4. Images of a glaucoma case with local deformations overlaid with the structure of the LC. For each view, the deformations at elevated IOP (left, up) and recovery (right, bottom) are represented.

Local Analysis: Maps of Deformation. Local deformations are seen as maps of deformations overlaid with the structure of the LC (Fig. 4). The arrows show different directions and different lengths which indicate parts of the structure expand while others contract. Interestingly, the whole LC is not deformed homogeneously, rather it is characterized by patterns of local deformations.

4 Conclusions

This paper describes the development of an image-based system to study the cause of glaucoma based on the hypothesis that rigidity of LC contributes to glaucomateous damage to axons. High resolution imaging of the LC structure requires the use of a prototype swept source OCT system. Whereas previous studies mostly reported assessment based on 2D methods on selected cross-sections, this is the first study to make full use of 3D imaging for measurements of pressure-induced deformations. The contribution of this work is a systematic approach to determine best performing methods which were tested and validated to overcome the challenges of image quality and patient and intra-ocular motions over longitudinal scans, moreover as pressure was induced to the eye via an external device. Given the clinical hypothesis and available OCT images from an experimental scanner, unbiased atlas-building was chosen to make best use

of the method's inherent capabilities, which include improved quality of the template and use of deformation maps to study global and local rigidity of the LC. Major efforts went into testing and validation, and the demonstration of feasibility in a small clinical study with three groups.

The proposed method captures subtle global and local structural changes in the LC under elevated IOP and recovery. The experimental setup and analysis method allows quantitative study of LC structure dynamics that has the potential to provide clinically useful biomarkers for glaucoma assessment.

Acknowledgements. This research was supported by NIH R01-EY013178 and EY025011.

References

1. Avants, B.B., Tustison, N., Song, G.: Advanced normalization tools (ANTs). Insight J. **2**, 1–35 (2009)
2. Dabov, K., Foi, A., Katkovnik, V., Egiazarian, K.: Image denoising by sparse 3-D transform-domain collaborative filtering. IEEE Trans. Image Process. **16**(8), 2080–2095 (2007)
3. Girot, C., Ishikawa, H., Fishbaugh, J., Wollstein, G., Schuman, J., Gerig, G.: Spatiotemporal analysis of structural changes of the lamina cribrosa. In: Cardoso, M.J., et al. (eds.) FIFI/OMIA-2017. LNCS, vol. 10554, pp. 185–193. Springer, Cham (2017). https://doi.org/10.1007/978-3-319-67561-9_21
4. Inoue, R., et al.: Three-dimensional high-speed optical coherence tomography imaging of lamina cribrosa in glaucoma. Ophthalmology **116**(2), 214–222 (2009)
5. Joshi, S., Davis, B., Jomier, M., Gerig, G.: Unbiased diffeomorphic atlas construction for computational anatomy. NeuroImage **23**, S151–S160 (2004)
6. Lee, E.J., Choi, Y.J., Kim, T.W., Hwang, J.M.: Comparison of the deep optic nerve head structure between normal-tension glaucoma and nonarteritic anterior ischemic optic neuropathy. PloS ONE **11**(4), e0150242 (2016)
7. Nadler, Z., et al.: In vivo three-dimensional characterization of the healthy human lamina cribrosa with adaptive optics spectral-domain optical coherence tomography. Invest. Ophthalmol. Vis. Sci. **55**(10), 6459–6466 (2014)
8. Ortiz, S., et al.: Optical distortion correction in optical coherence tomography for quantitative ocular anterior segment by three-dimensional imaging. Opt. Express **18**(3), 2782–2796 (2010)
9. Quigley, H.A., Broman, A.T.: The number of people with glaucoma worldwide in 2010 and 2020. Br. J. Ophthalmol. **90**(3), 262–267 (2006)
10. Sigal, I.A., Wang, B., Strouthidis, N.G., Akagi, T., Girard, M.J.: Recent advances in OCT imaging of the lamina cribrosa. Br. J. Ophthalmol. **98**(Suppl 2), ii34–ii39 (2014)
11. Unser, M., Aldroubi, A., Eden, M.: Fast B-spline transforms for continuous image representation and interpolation. IEEE Trans. Patt. Anal. Mach. Intell. **13**(3), 277–285 (1991)
12. Wollstein, G., et al.: Optical coherence tomography longitudinal evaluation of retinal nerve fiber layer thickness in glaucoma. Arch. Ophthalmol. **123**(4), 464–470 (2005)